Ising-like antiferromagnetism on the octahedral sublattice of a cobalt-containing garnet and the potential for quantum criticality

Abbey J. Neer, JoAnna Milam-Guerrero, Justin E. So, and Brent C. Melot*
Department of Chemistry, University of Southern California, Los Angeles, California 90089-1062, USA

Kate A. Ross
Department of Physics, Colorado State University, Fort Collins, Colorado 80523-1875, USA

Zeric Hulvey
NIST Center for Neutron Research, Gaithersburg, Maryland 20899-8562, USA
and Department of Materials Science and Engineering, University of Maryland, College Park, Maryland 20742, USA

Craig M. Brown
NIST Center for Neutron Research, Gaithersburg, Maryland 20899-8562, USA

Alexey A. Sokol
Department of Chemistry, Kathleen Lonsdale Materials Chemistry, University College London, 20 Gordon Street, London WC1H 0AJ, United Kingdom

David O. Scanlon
Department of Chemistry, Kathleen Lonsdale Materials Chemistry,
University College London, 20 Gordon Street, London WC1H 0AJ, United Kingdom
and Diamond Light Source Ltd., Diamond House, Harwell Science and Innovation Campus, Didcot, Oxfordshire OX11 0DE, United Kingdom
(Received 17 August 2016; revised manuscript received 5 March 2017; published 14 April 2017)

In this contribution, we report that $CaY_2Co_2Ge_3O_{12}$ exhibits an unusual anisotropic and chainlike antiferromagnetic arrangement of spins despite crystallizing in the highly symmetric garnet structure. Using low-temperature powder neutron diffraction and symmetry analysis, we identify a magnetic structure consisting of chainlike motifs oriented along the body diagonals of the cubic unit cell with moments pointing parallel to the chain direction due to the strong Ising character of the Co ions. Antiferromagnetic order sets in below 6 K and exhibits both temperature- and field-induced magnetic transitions at high fields. Combining the results, we present a magnetic phase diagram that suggests $CaY_2Co_2Ge_3O_{12}$ undergoes a quantum phase transition at low temperatures and moderate fields.

DOI: 10.1103/PhysRevB.95.144419

The garnet structure, with general composition $R_3B_2(AO_4)_3$, has been called the "fruit fly of magnetism" because the rich compositional diversity is ideal for developing fundamental knowledge about magnetic interactions in the solid state [1]. The eponymous mineral adopts the cubic space group $Ia\bar{3}d$ (No. 230) and consists of a 3D network of BO_6 octahedra that share corners with bridging AO_4 tetrahedra, as illustrated in Fig. 1(a). This connectivity also creates an eight-coordinate interstitial where larger cations like the rare earths can sit in a distorted cubic (8-coordinate) environment, as represented by the black spheres in Fig. 1(a).

Unlike other structural families, such as the perovskites or spinels, garnets cannot be easily described in terms of close-packed ionic spheres. Instead, Andersson and O'Keefe have developed a description based on the tight packing of cylinders [2]. Within this picture, the oxygen anions sit around each of the four threefold axes of rotation that run along the body diagonals of the cubic unit cell. This symmetry creates rods out of the octahedral sites that are then joined together by vacant triangular prisms that are formed from the faces of the cubic sites [Fig. 1(c)]. Three of these rods [colored blue, red, and purple in Fig. 1(c)] run at angles around a central one and cross within the plane without intersecting [Fig. 1(b)].

This unique topology motivated us to investigate how magnetic ions with strong single-ion anisotropy would behave when decorating these rods. Using low-temperature powder neutron diffraction combined with magnetic susceptibility and heat capacity measurements, we have studied $CaY_2Co_2Ge_3O_{12}$ and found the system to adopt a fairly unusual ordered state that is best visualized as antiferromagnetic chains of spins oriented along the body diagonals. We also find evidence that suggests a quantum phase transition occurs near a magnetic field of 6 T.

We began our study by using powder neutron diffraction to determine the low-temperature magnetic structure. Data were collected on the high resolution powder diffractometer, BT-1, at the NIST Center for Neutron Research and the nuclear and magnetic structure were refined against the data using the Rietveld method [3] as implemented in the FULLPROF software suite, [4] with the resulting parameters given in Supplemental Material Table I [5]. The room temperature

*melot@usc.edu

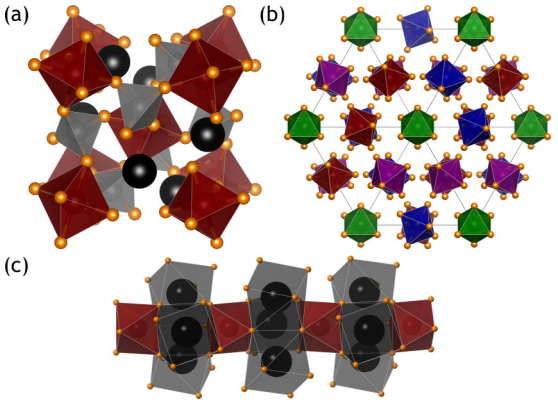

FIG. 1. (a) First quadrant of the garnet unit cell showing the tetrahedral sites in gray, octahedral sites in red, and cubic sites as black spheres. (b) Illustration of the rod packing first described by Andersson and O'Keefe. The projection of the structure is shown such that the four rods, each uniquely colored and isolated in (c), are most visible.

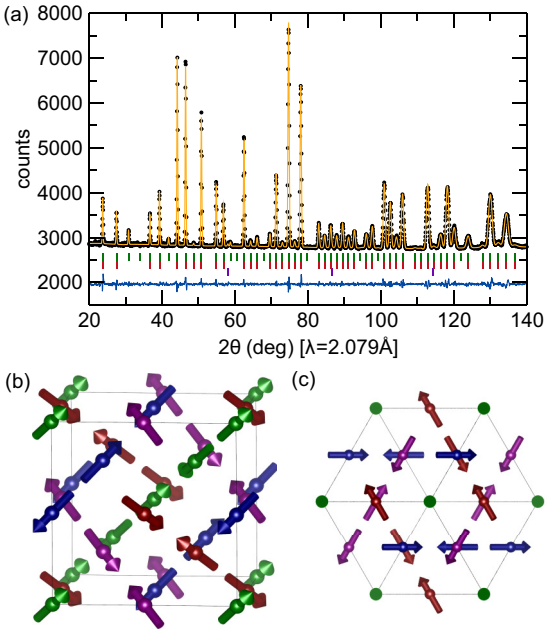

FIG. 2. (a) Results of the Rietveld refinement against the 2 K powder neutron diffraction data. $R^{nuc}_{Bragg} = 1.5\%, R_{mag} = 8.5\%$. (b) Illustration of the resulting magnetic structure viewed off one of the cubic unit cell edges. (c) Projection illustrating the magnetic structure down the (111) axis of the unit cell. In both illustrations the spins are color coded to match the octahedral rods in Fig. 1.

nuclear structure was found to be in good agreement with the cubic $Ia\bar{3}d$ structure with Co ions located on the octahedrally coordinated 16*a* site. In order to fit the reflections associated with the onset of magnetic order observed at 23.8°, 30.8°, 36.7°, 41.8°, and 58.7° in the 2 K patterns, the method of representational analysis was used. All reflections could be indexed using a simple wave vector of $\mathbf{k} = 0$, with the BasiReps routine within FULLPROF returning four one-dimensional, two two-dimensional, and four three-dimensional representations within the Little group G_k.

A reasonable fit of the diffraction data, shown in Fig. 2(a), could only be obtained using the first representation, Γ_1, which consists of the basis vectors listed in Supplemental Material Table II [5]. This representation corresponds to the magnetic space group $Ia\bar{3}d$ and requires the moments point along the body diagonals of the unit as illustrated in Figs. 2(b) and 2(c). The refined moment resulting from the fit was 2.7(1) μ_B per Co, consistent with magnetization measurements and point-charge calculations, as will be discussed in detail below.

The irreducible representation that best describes the magnetic structure, illustrated in Figs. 2(b) and 2(c), constrains the spins to point along the body diagonals of the cubic unit cell and, as a result, orients the moments along the long axis of the octahedral chains that Andersson and O'Keefe described. This type of order contrasts with other garnets, like $Ca_3Cr_2Ge_3O_{12}$, which has been reported to possess ferromagnetic layers of spins that couple antiferromagnetically to each other in a more conventional manner [6,7]. This can most likely be attributed to the fact that octahedrally coordinated Co^{2+} can be characterized using a $j_{\text{eff}} = 1/2$ description because of the interplay of spin-orbit coupling and the crystal electric field (CEF). The single ion ground state is a Kramers doublet, often separated by ~30 meV (~300 K) from the next excited level [8–11]. The $j_{\text{eff}} = 1/2$ moment formed by the single ion ground state doublet acquires anisotropy in a distorted octahedron and must be described by anisotropic *g* tensor. The oxygen environment of Co^{2+} in $CaY_2Co_2Ge_3O_{12}$ is trigonally distorted (point group S_6), with the octahedron being elongated along a local [111] direction, the same directions that define the structural "rods." For Co^{2+}, this type of distortion generically produces an Ising-like *g* tensor, and for $CaY_2Co_2Ge_3O_{12}$, the Ising direction is consistent with the refined magnetic structure shown in Fig. 2.

To estimate the *g*-tensor anisotropy in $CaY_2Co_2Ge_3O_{12}$, a point charge calculation was carried out following the method of Hutchings [12] to obtain the CEF Hamiltonian. This was simultaneously diagonalized with the spin orbit coupling Hamiltonian within the full 28×28 $|L_z, S_z\rangle$ basis of the ^{4}F free ion term for Co^{2+}, yielding *g*-tensor components $g_z = 5.7$ and $g_{xy} = 3.9$. These results are in good agreement with the observed moment determined from neutron diffraction, since $\mu_z = \frac{1}{2} g_z = 2.85\ \mu_B$, which compares well with the refined ordered moment of 2.7 μ_B at $T = 2$ K. In a low energy effective theory with interactions between these $j_{\text{eff}} = 1/2$ moments, this Ising-like *g* tensor would be projected into the effective exchange interactions, producing an Ising-like exchange Hamiltonian [10,13–15].

The temperature-dependent magnetic susceptibility, shown in Fig. 3(a), indicates that the spins establish this antiferromagnetic ground state starting around 6 K. Fitting the high temperature region (200–300 K) of the magnetic susceptibility to the Curie-Weiss equation, $\chi = C/(T - \Theta_{CW})$, provides some insight into the mean-field average of the magnetic interactions. The effective moment per Co^{2+} was found to be 5.17 μ_B, in close agreement with the expected value of 5.2 μ_B in a high spin octahedral coordination environment where the contributions from the spin and orbital components of the magnetization are fully decoupled ($\mu_{(L+S)} = \sqrt{4S(S+1) + L(L+1)}$). The Θ_{CW} was found to be −35 K,

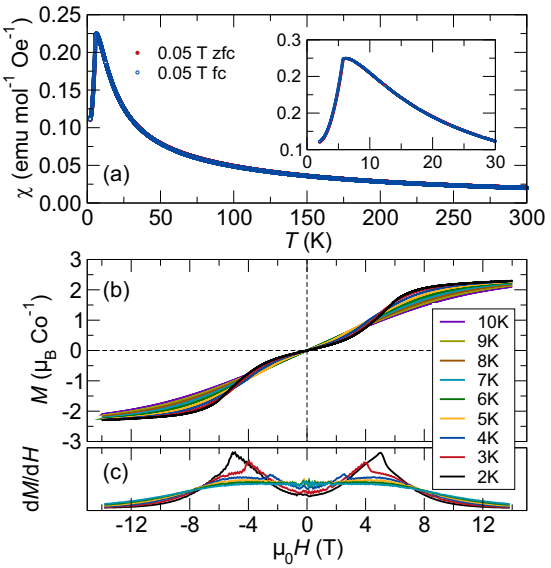

FIG. 3. (a) Temperature-dependent susceptibility of $CaY_2Co_2Ge_3O_{12}$ collected with a field of 500 Oe. The inset emphasizes the cusp associated with the onset of antiferromagnetic order around 6 K. (b) Isothermal magnetization curves collected through the magnetic ordering transition. (c) Derivative of the magnetization with respect to the applied field after smoothing with a running average of ten points for clarity. Note the temperature dependence of the field induced transition that occurs around 6 T in the 2 K data.

reflecting that a moderate antiferromagnetic coupling appears to dominate the interactions within the octahedral sublattice. Care should be exercised when interpreting the Curie-Weiss data, however, since the temperature range over which the fits are performed is approaching the energy of the first excited single-ion level (see Supplemental Material [5]).

Given that neighboring octahedral sites do not share any common bonds, the interactions will be heavily influenced by the ions on the cubic and tetrahedral positions. These superexchange pathways typically consist of Co-O-(A/R)-O-Co linkages or super-superexchange along the edge of the polyhedra in a way similar to the A-site magnetic spinels like $CoAl_2O_4$ and $FeSc_2S_4$ [16–20]. The preference for antiferromagnetic order along the rods suggests that the pathway through the cubic site, which couples spins along the length of the rods, dominates over the tetrahedral pathways that bridge the neighboring chains. While long pathways such as this are often very weak, the influence of the intrachain superexchange is strengthened by the 12-fold degeneracy of the linkages and the shorter Co-Co distance along the rod (5 Å) compared to the interchain distance (6 Å).

The effects of magnetic coupling were further examined with *ab initio* periodic density functional theory using a noncollinear spin model so that the anisotropy along the body diagonals could be evaluated. It is important to note that the inclusion of spin-orbit interactions and a careful calibration of the initial spin directions in the self-consistent field procedure is essential to build a realistic picture of the ground and excited states. Crucially, the real spin distribution across the unit cell and atomic relaxations are included into the calculation of the magnetic coupling constants.

The procedure was based on a delta self consistent field (SCF) method, in which the strength of a particular interaction was estimated from energy differences between different states of the system of interest. In the current case, we configured the system to adopt the experimentally observed antiferromagnetic chains along the principal diagonals of the unit cell in the ground state of $CaY_2Co_2Ge_3O_{12}$ ($+-+-$). We then introduced local perturbations into the system, which would correspond to highly localized spin waves, in the form of (i) one ferromagnetically ordered chain per unit cell ($++++$), and (ii) a ferromagnetically ordered chain with one "defect" ($+++-$). The SCF iterations in each case preserved the initial trial spin directions but led to noticeable spin density readjustment followed by atomic relaxations thus reducing the energy penalty of the spin flip. Mapping the difference in total energies of these three configurations onto a Hamiltonian describing two magnetic sublattices of $\frac{3}{2}\hbar$ spins, the nearest neighbor, J_1, and the next-nearest-neighbor along the chain, J_2, coupling constants were calculated to be 23 K and 9 K, respectively, with an estimated error of less than 1 K. It is interesting to note that the relatively high value of J_2 ($\sim\frac{1}{3}J_1$) implies that longer-range next-nearest-neighbor interactions are certainly non-negligible and should produce magnetic excitations on heating that disrupt the ground state order.

Having thoroughly evaluated the zero field ground state, isothermal magnetization curves were collected at a variety of temperatures between 10 K and 2 K to assess the stability of the magnetic order against external perturbations [Fig. 3(b)]. For small applied fields, the usual linear response expected from a well-ordered antiferromagnet can be clearly seen at all temperatures. Starting at 4 K, however, a distinct field-dependent magnetic transition begins to evolve around 25 kOe, which moves to fields of 40 kOe and 50 kOe as the temperature is decreased further. Field-dependent metamagnetic transitions such as this have been observed in several other Co-based compounds [21–23] and are typically attributed to the magnetic field strength becoming strong enough to overcome the single-ion anisotropy of the moments and drive the order towards a field polarized state [21,22].

The field and temperature dependence of the magnetism encouraged us to explicitly map out these transitions using specific heat measurements as shown in Fig. 4(a). In the absence of a magnetic field, a sharp lambdalike anomaly evolves at 6 K, in very good agreement with the temperature-dependent magnetic susceptibility data. As lambda anomalies are not expected for purely one-dimensional materials, due to the lack of long-range magnetic order [24], the system clearly undergoes a three-dimensional transition despite the highly anisotropic character of the magnetic structure.

As increasing field strengths are applied, the peak in the heat capacity is continuously suppressed until a field of 6 T, past which point the peak reverses trend and begins increasing in temperature. In these large fields, the features in the specific heat begin to resemble the kind of broad peaks typically associated with a disordered state [Fig. 4(e)]. Similar behavior has been seen in the transverse field Ising model material $CoNb_2O_6$ after it passes through its quantum critical

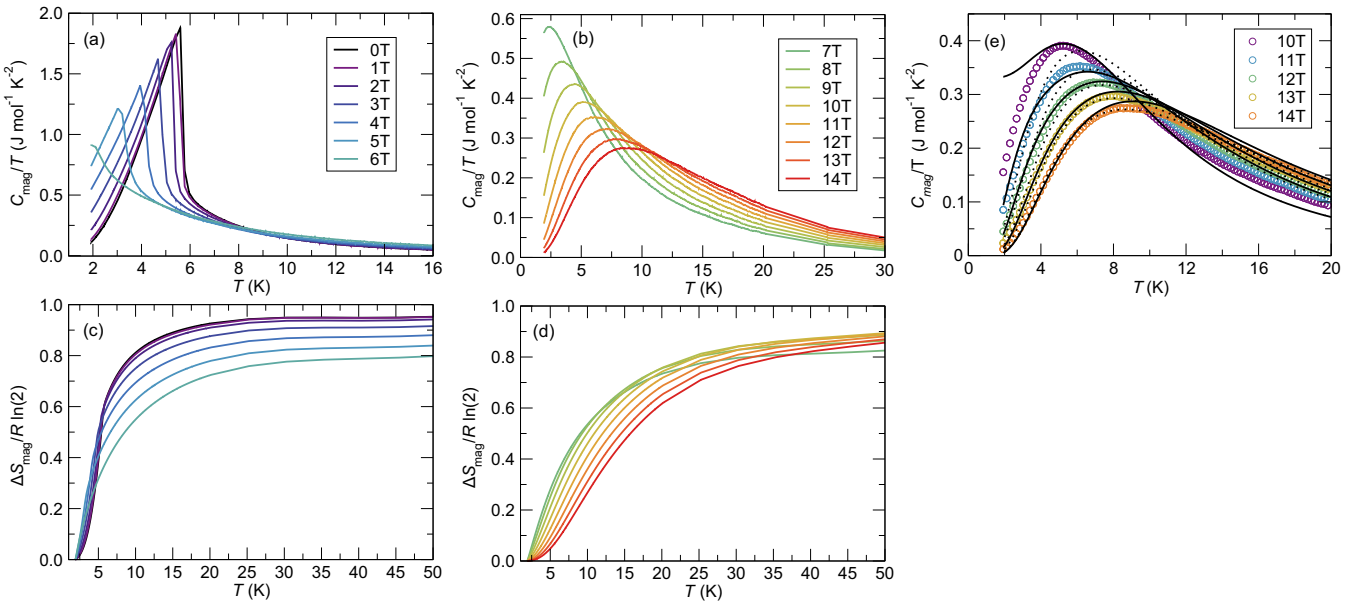

FIG. 4. Magnetic contribution to the specific heat at (a) low and (b) high field strengths. The lattice contribution was approximated by separately measuring and subtracting the specific heat of $CaY_2Mg_2Ge_3O_{12}$ in order to estimate the change in entropy associated with the onset of magnetic order in (c) low and (d) high fields, normalized to the maximum value of $R\ln(2)$. (e) Fits to the heat capacity using the free fermion (solid black line) and Schottky model (dashed black line) discussed in the text.

point [25–27], suggesting that $CaY_2Co_2Ge_3O_{12}$ transitions into a field polarized paramagnetic state around this point. Correlating the specific heat with the sharp upturn in the magnetization curves supports the notion that the compound is transitioning from the antiferromagnetic ground state into a new phase with a much larger concentration of uncompensated moments.

Attempts to fit the data using the free-fermion model of Pfeuty [27], which describes the behavior of a one-dimensional chain of Ising spins, were performed by starting with the coupling constants determined from the DFT calculations. It was found that fixing a value of $J = 23$ K failed to produce a satisfactory fit; however, good agreement was obtained with a value of 27 K as illustrated in Fig. 4(e). This discrepancy may be attributed to the artificial cation order that is necessary in the computational cell, the presence of interchain interactions, or from nontransverse components of the applied field, but still represents a good first approximation. Within the free fermion model, there are two important parameters: the exchange coupling, J, and Γ, a parameter used to estimate the extent of the disorder within the system, with a table of fitted values given in Supplemental Material Table III [5,27]. In our fits, J was held constant while Γ was optimized using a least-squares fitting algorithm. Importantly, all of our fitted values of Γ are greater than $J/2$, indicative of a fully disordered system, confirming the paramagnetic state above 10 T.

The disruption to the long-range ordered state was further verified by fitting the heat capacity data in high fields (μ_0 H = 14 T) to a powder-averaged 2-state (Schottky) model with an anisotropic g tensor [Fig. 4(e)]. The heat capacity for the other field strengths was then calculated based upon this fit. We averaged the heat capacity response over all possible field orientations, as well as the four local coordinate systems appropriate to the four types of Ising chains in the lattice. The extracted values for g_{xy} and g_z are in rough agreement with the calculations based on the point charge model discussed above; $g_{xy} = 1.844 +/- 0.005$ and $g_z = 6.26 +/- 0.02$ (Schottky model) vs $g_{xy} = 3.9$ and $g_z = 5.7$ (point charge). Disagreement between these two approximations is expected. Point charge calculations often do not produce quantitatively accurate results, but are useful for generally reproducing the qualitative features of the single-ion anisotropy. Meanwhile, the Schottky model considers just the Zeeman splitting of the $j_{\text{eff}} = 1/2$ moments and thus assumes no interactions between them. The single-ion approximation inherent in the Schottky model should become more valid in the high field limit, however the g values will become renormalized due to field-induced mixing with the higher single-ion levels. The two methods, however, do agree on the overall Ising-like nature of the moments, which provides a natural explanation for the existence of a quantum critical point in this material.

Combining the specific heat and magnetization data, the field dependence of the transition temperature can be used to map out the magnetic phase diagram illustrated in Fig. 5. The transition to the antiferromagnetic ground state shows a continuous suppression of T_N that can be fit with a 1-aH_c^2 dependence that extrapolates to the complete suppression of antiferromagnetism to 0 K around 7.5 T. The dashed red line represents a linear fit as a guide to the eye. This phase diagram strongly suggests that the material undergoes a quantum phase transition with a critical field between 6 T and 7.5 T. If this high field transition is indeed a critical point, the red region in Fig. 5 corresponds to a field-polarized paramagnetic state. In proximity of the phase transition, quantum fluctuations will dominate the behavior of the system which could explain the difficulty in fitting specific heat data collected near these fields.

Considering the highly anisotropic arrangement of Ising-like moments, this material is reminiscent of the transverse

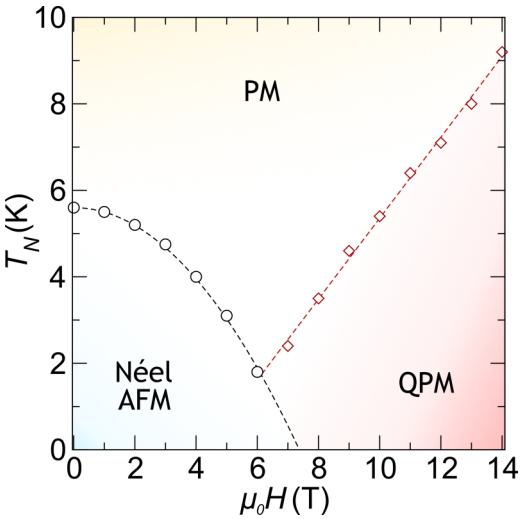

FIG. 5. Magnetic phase diagram of the garnet $CaY_2Co_2Ge_3O_{12}$ suggesting the presence of a quantum critical point when exposed to fields around 6 T. The open black circles were extracted as the peak position of the lambda anomaly while the open red diamonds represent the maxima of the broad feature in the disordered phase. AFM = antiferromagnet, PM = thermally disordered paramagnet, QPM = field polarized quantum paramagnet.

field Ising model, which is normally associated with $CoNb_2O_6$ or $LiHoF_4$. Yet, unlike these compounds, the orientation of the moments in $CaY_2Co_2Ge_3O_{12}$ do not have a global direction that is transverse to the Ising axis. This means that, even in a single crystal sample, the field will always create a longitudinal field on some of the sublattices. Furthermore our simple estimate of the g tensor suggests that the model would not be strictly Ising but rather of an XXZ type with dominant Ising effective exchange interactions between $j_{\text{eff}} = 1/2$ moments. Dmitriev and coworkers have described such a case in a recent report [28] and find, despite the introduction of a longitudinal field component, that Ising chains should still exhibit a critical point similar to what we see here, supporting the one-dimensional Ising character of the garnet.

In summary, we have investigated the magnetic properties of the garnet $CaY_2Co_2Ge_3O_{12}$ and found a complex antiferromagnetic ground state that is strongly influenced by the presence of external magnetic fields. Our results suggest that despite a 3D crystal structure, the magnetic interactions along chains are dominant. The Ising-like magnetocrystalline anisotropy of Co^{2+} suggests that and effective exchange Hamiltonian between $j_{\text{eff}} = 1/2$ moments incorporating Ising or weak XXZ character may be appropriate. Many questions remain regarding the nature of the magnetic excitations in the proposed quantum critical region of the phase diagram as the effect of field orientation with respect to the individual chains. The growth of single crystal samples and neutron spectroscopy will be critical for addressing many of these questions and furthering our understanding of the field- and temperature-dependent properties of this novel cobalt-based garnet.

A.J.N., J.M.G., J.S., and B.C.M. gratefully acknowledge support from the Office of Naval Research Grant No. N00014-15-1-2411 and fruitful discussions with Stephen Wilson at UC Santa Barbara. Computational work in this paper used the UCL Grace HPC Facility and the Archer UK National Supercomputing Service, which was accessed through the UK's HEC Materials Chemistry Consortium, funded by EPSRC (EP/L000202). The work at UCL was supported by EPSRC (EP/N01572X/1). D.O.S. and A.A.S. acknowledge J. A. B. Buckeridge and C. R. A. Catlow for many useful discussions. We acknowledge the support of the National Institute of Standards and Technology,U. S. Department of Commerce, in providing the neutron research facilities used in this work.

[1] P. E. Wigen, R. D. McMichael, and C. Jayaprakash, J. Magn. Magn. Mater. **84**, 237 (1990).
[2] M. O'Keeffe and S. Andersson, Acta Crystallogr. Sect. A **33**, 914 (1977).
[3] H. M. Rietveld, J. Appl. Cryst. **2**, 65 (1969).
[4] J. Rodríguez-Carvajal, Physica B **192**, 55 (1993).
[5] See Supplemental Material at http://link.aps.org/supplemental/10.1103/PhysRevB.95.144419 for details of the structural parameters from the Rietveld refinement.
[6] W. Prandl, Solid State Commun. **10**, 529 (1972).
[7] A. Meyer, W. F. Perger, R. Demichelis, B. Civalleri, and R. Dovesi, Int. J. Quantum Chem. **110**, 2192 (2010).
[8] A. Abragam and B. Bleaney, *Electron Paramagnetic Resonance of Transition Ions* (OUP, Oxford, 2012).
[9] W. Buyers, T. Holden, E. Svensson, R. Cowley, and M. Hutchings, J. Phys. C **4**, 2139 (1971).
[10] J. P. Goff, D. A. Tennant, and S. E. Nagler, Phys. Rev. B **52**, 15992 (1995).
[11] K. A. Ross, J. M. Brown, R. J. Cava, J. W. Krizan, S. E. Nagler, J. A. Rodriguez-Rivera, and M. B. Stone, arXiv:1703.07468.
[12] M. T. Hutchings, Solid State Phys. **16**, 227 (1964).
[13] M. E. Lines, Phys. Rev. **131**, 546 (1963).
[14] R. M. White, *Quantum Theory of Magnetism: Magnetic Properties of Materials* (Springer-Verlag, Berlin, Heidelberg, 2007).
[15] S. Guitteny, S. Petit, E. Lhotel, J. Robert, P. Bonville, A. Forget, and I. Mirebeau, Phys. Rev. B **88**, 134408 (2013).
[16] B. C. Melot, K. Page, R. Seshadri, E. M. Stoudenmire, L. Balents, D. L. Bergman, and T. Proffen, Phys. Rev. B **80**, 104420 (2009).
[17] N. Tristan, J. Hemberger, A. Krimmel, H.-A. Krug von Nidda, V. Tsurkan, and A. Loidl, Phys. Rev. B **72**, 174404 (2005).
[18] G. Blasse, Philips Res. Repts. **18**, 383 (1963).
[19] V. Fritsch, J. Hemberger, N. Büttgen, E.-W. Scheidt, H.-A. Krug von Nidda, A. Loidl, and V. Tsurkan, Phys. Rev. Lett. **92**, 116401 (2004).
[20] G. Chen, L. Balents, and A. P. Schnyder, Phys. Rev. Lett. **102**, 096406 (2009).
[21] B. C. Melot, B. Paden, R. Seshadri, E. Suard, G. Nénert, A. Dixit, and G. Lawes, Phys. Rev. B **82**, 014411 (2010).

[22] B. C. Melot, A. Goldman, L. E. Darago, J. D. Furman, E. E. Rodriguez, and R. Seshadri, J. Phys.: Condens. Matter **22**, 506003 (2010).
[23] J. R. Neilson, B. C. Melot, D. P. Shoemaker, J. A. Kurzman, and R. Seshadri, D. E. Morse, Phys. Rev. B **83**, 094418 (2011).
[24] A. Tari, *The Specific Heat of Matter at Low Temperatures (Hardcover)* (Imperial College Press, London, 2003).
[25] T. Liang, S. M. Koohpayeh, J. W. Krizan, T. M. McQueen, R. J. Cava, and N. P. Ong, Nat. Commun. **6**, 7611 (2015).
[26] E. Lieb, T. Schultz, and D. Mattis, Ann. Phys. **16**, 407 (1961).
[27] P. Pfeuty, Ann. Phys. **57**, 79 (1970).
[28] A. A. Ovchinnikov, D. V. Dmitriev, V. Y. Krivnov, and V. O. Cheranovskii, Phys. Rev. B **68**, 214406 (2003).